



Contents lists available at ScienceDirect

Journal of Volcanology and Geothermal Research

journal homepage: www.elsevier.com/locate/jvolgeores



The 6–8 Aug 2019 eruption of ‘Volcano F’ in the Tofua Arc, Tonga

Philipp A. Brandl^{a,*}, Florian Schmid^a, Nico Augustin^a, Ingo Grevemeyer^a,
Richard J. Arculus^b, Colin W. Devey^a, Sven Petersen^a, Margaret Stewart^c, Heidrun Kopp^a,
Mark D. Hannington^{a,c}

^a GEOMAR Helmholtz Centre for Ocean Research Kiel, Wischhofstr. 1-3, 24148 Kiel, Germany

^b Research School of Earth Sciences, The Australian National University, 142 Mills Road, Acton ACT 2601, Australia

^c Department of Earth and Environmental Sciences, University of Ottawa, 25 Templeton Street, Ottawa, Ontario K1N 6N5, Canada

ARTICLE INFO

Article history:

Received 13 September 2019

Received in revised form 23 October 2019

Accepted 28 October 2019

Available online xxx

Keywords:

Tonga

Tofua Arc

Submarine eruption

Pumice raft

Island arc

ABSTRACT

In August 2019 a large raft of pumice appeared in the territorial waters of Tonga. As in many other cases, this pumice raft was the only surface expression of a major submarine volcanic eruption. Discolored water and reconstruction of the drift path of the pumice raft using satellite imagery points towards ‘Volcano F’ in the Tofua Arc NW of the island of Vava'u as the most likely volcanic source. Here we present imagery from ESA's Sentinel-2 satellite that captured the start of the submarine eruption on 6 August 2019 and the waning of the eruption on 8 August, followed by observations of the drifting pumice raft until 14 August. This start time is consistent with T-phase records at the seismic stations on Niue Island and Rarotonga and the signal delay time of 733 s between the two stations is consistent with an origin at or at least near Volcano F. On 8 August, a $>136.7 \text{ km}^2$ large raft of pumice appears at the sea surface. The modelled minimum raft volume is $8.2\text{--}41.0 \times 10^6 \text{ m}^3$, which is equivalent to $2.5\text{--}12.3 \times 10^6 \text{ m}^3$ dense rock. The eruption thus corresponds to a volcanic explosivity index (VEI) 2–3 eruption in the submarine environment. Prior to the volcanic eruption, a series of earthquakes close to Volcano F was recorded. The series started on 5 August with a Mb 4.7 event, followed by at least six shallow earthquakes (Mb >3.9) on 6 August. In December 2018 and January 2019, we surveyed the seafloor around Volcano F with multibeam sonar. Combining our data with pre-existing information, we present the first comprehensive bathymetric map of the volcanic edifice and its geologic setting. We show that Volcano F represents a major arc volcanic complex that is situated in an extensional setting. The basal diameter of the volcanic apron is $>50 \text{ km}$ with a large central, $8.7 \times 6 \text{ km}$ caldera with a floor at $\sim 700 \text{ m}$ water depth. The top of the post-caldera constructional cone complex had a summit depth of 35 m below sea level in 2004. The volcano shows geochemical differences to the adjacent arc volcanoes on Fonualei and Late islands. The volcano's pristine volcanic morphology and two documented eruptions (2001 and 2019) indicate a highly active volcanic system that warrants further scientific attention.

© 2019 Elsevier B.V. All rights reserved.

1. Introduction

The annual magma budget of the Earth is dominated by melt generated at mid-ocean ridges. However, continental and island arc magmatism represent the second largest contribution to terrestrial magmatism (cf. Crisp, 1984). Melting at these magmatic arcs is driven by the subduction of lithosphere and the devolatilization of the slab at depth. The released fluids trigger melting in the overlying convecting mantle wedge and the resulting ascending arc magmas are volatile-rich. Volatile load and a thick crust at magmatic arcs

enhance magmatic differentiation and drive arc rocks to compositions generally much more viscous and silicic than at mid-ocean ridges. Thus, arc volcanoes erupt in various styles ranging from effusive to catastrophically explosive. Volcanic eruptions and/or sector collapses of composite arc volcanoes represent a major hazard but any comprehensive risk assessment is complicated by the fact that many magmatic arcs are intra-oceanic with arc volcanoes often submerged. This also applies to the $>2,500 \text{ km}$ -long Tofua-Kermadec Arc in the Southwest Pacific, where only a few volcanoes rise above sea-level (Fig. 1A). Marine surveys in the late 1980s and 1990s provided evidence for the high magmatic productivity of the Tofua-Kermadec Arc (Smith and Price, 2006).

Since 1774, a total of 77 volcanic eruptions have been recorded from the Tongan section of the Tofua-Kermadec Arc alone (Global

* Corresponding author.

E-mail address: pbrandl@geomar.de (P.A. Brandl).

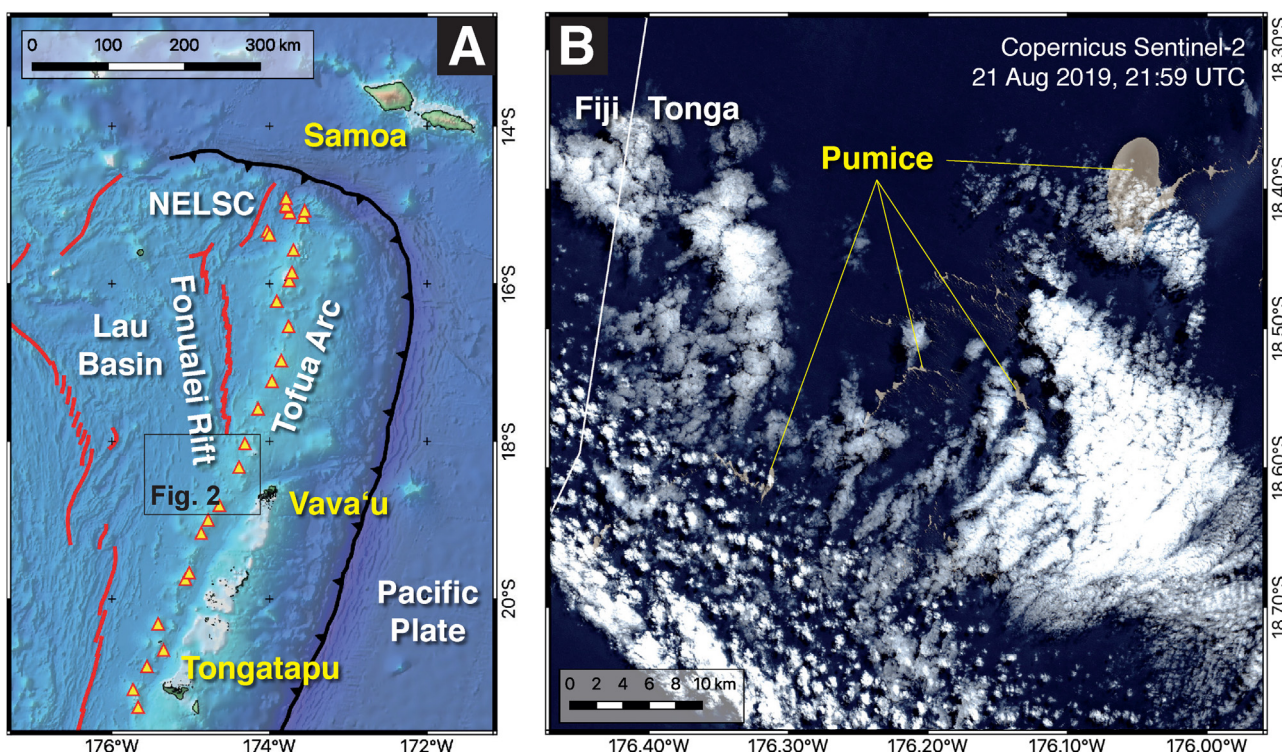


Fig. 1. A) Overview map of the Tofua Arc. Arc volcanoes are shown by yellow triangles, spreading centers by red lines and the Tonga subduction zone by the black line with triangles. B) Sentinel-2 satellite image of the pumice raft close to the maritime border between Fiji and Tonga on 21 August 2019 (image contains modified Copernicus Sentinel data 2019). (For interpretation of the references to colour in this figure legend, the reader is referred to the web version of this article).

(Volcanism Program, 2013). However, direct observations of historical submarine volcanic activity remain scarce except for frequent but small eruptions at the Monowai volcanic center (e.g., Chadwick et al., 2008; Wright et al., 2008; Watts et al., 2012; Metz et al., 2016, 2019) and direct observations of the 2009 boninite eruption at West Mata by submersible (Resing et al., 2011) and subsequent periodic remapping (Chadwick, 2019). Besides direct visual observations, seismoacoustic T-phases allow volcanic eruptions to be detected over distances of several thousands of kilometers because this signal is coupled into the SOFAR channel (cf. Metz et al., 2016). In many cases, however, pumice rafts floating at the sea surface are the only evidence for recent submarine, silicic eruptions; Continuous Earth observation from space allow to track these rafts and trace them back to their initial volcanic source. Previously, there were ten major submarine eruptions recorded from the Tofua-Kermadec Arc that produced large pumice rafts (see compilation of Bryan et al., 2012 plus the 2012 eruption of Havre: Jutzeler et al., 2014). These include the 1967 and 1979 eruptions of Metis Shoal (Bryan et al., 2012), the 1984 and 2006 eruptions of Home Reef (Vaughan et al., 2007; Mantas et al., 2011; Bryan et al., 2012), the 2001 eruption (Bryan et al., 2004) of the unnamed volcano #243091 (Global Volcanism Program, 2013; listed as #0403-091 in Bryan et al., 2004), and the 2012 eruption of Havre (Jutzeler et al., 2014; Carey et al., 2018). In August 2019, reports of a large pumice raft observed in the territorial waters of Tonga and drifting westwards (Fig. 1B) triggered our interest because we surveyed the area of the suspected volcanic source during RV Sonne cruise SO-267 (Archimedes I) in December 2018 to January 2019 (Hannington et al., 2019). In this manuscript we summarize existing information and present new constraints on the August 2019 submarine eruption in the Tofua Arc of Tonga integrating data from remote sensing, seismology, hydroacoustic surveying and geological sampling. Our aim is to provide a robust framework for future detailed studies of what we think is a highly active yet largely unexplored submarine arc volcano.

2. The August 2019 submarine eruption in Tonga

On 15 August 2019, sailing boats encountered a large pumice raft about 75 km west of Late Island, an active island arc volcano in the Tofua Arc of Tonga (Fig. 2). Sulfur smell was present and the floating layer of pumice reached up to 30 cm in thickness with individual pieces up to 80 cm in diameter (see detailed report by Sail Surf ROAM: <https://www.facebook.com/sailsurfroam/posts/30459493420876170>; Global Volcanism Program, 2019). However, based on satellite imagery from NASA (<https://worldview.earthdata.nasa.gov>; accessed on 29 August 2019), the pumice raft first appeared on 8 August in a rear-arc location between the volcanic islands of Fonualei and Late (Fig. 2). Daily satellite observation and good visibility (i.e. little cloud cover) allow the pumice raft to be tracked over the corresponding time period, demonstrating that the pumice raft encountered on 15 August is the same that was spotted on satellite imagery from 8 August (Fig. 2). A large plume of discolored water is also visible on the images from 8 August and stretches from a then-unnamed submarine volcano located in the arc front between Fonualei and Late islands and an unnamed submarine volcano in the rear-arc (Fig. 2). The submarine arc volcano is listed as #243091 in the database of the Global Volcanism Program (2013) and was the source of a previous pumice-raft producing eruption on 27–28 September 2001 (Bryan et al., 2004; Global Volcanism Program, 2019). This volcano was first mapped during RV Southern Surveyor cruise SS2004/11 (Northern Tonga Vents Expedition ‘NoToVE’) in 2004 and is listed as ‘Volcano F’ in the corresponding cruise summary (Arculus and SS2004/11 shipboard scientists, 2004). In this manuscript we will use Volcano F as the name of the volcano. The volcano to the west of Volcano F that is in the center of the pumice raft on 8 August (Fig. 2) is extinct based on field observations during SO-267 (low backscatter, dredged altered volcanics and carbonates) and we thus suspect Volcano F in the arc front as the most likely site of eruption.

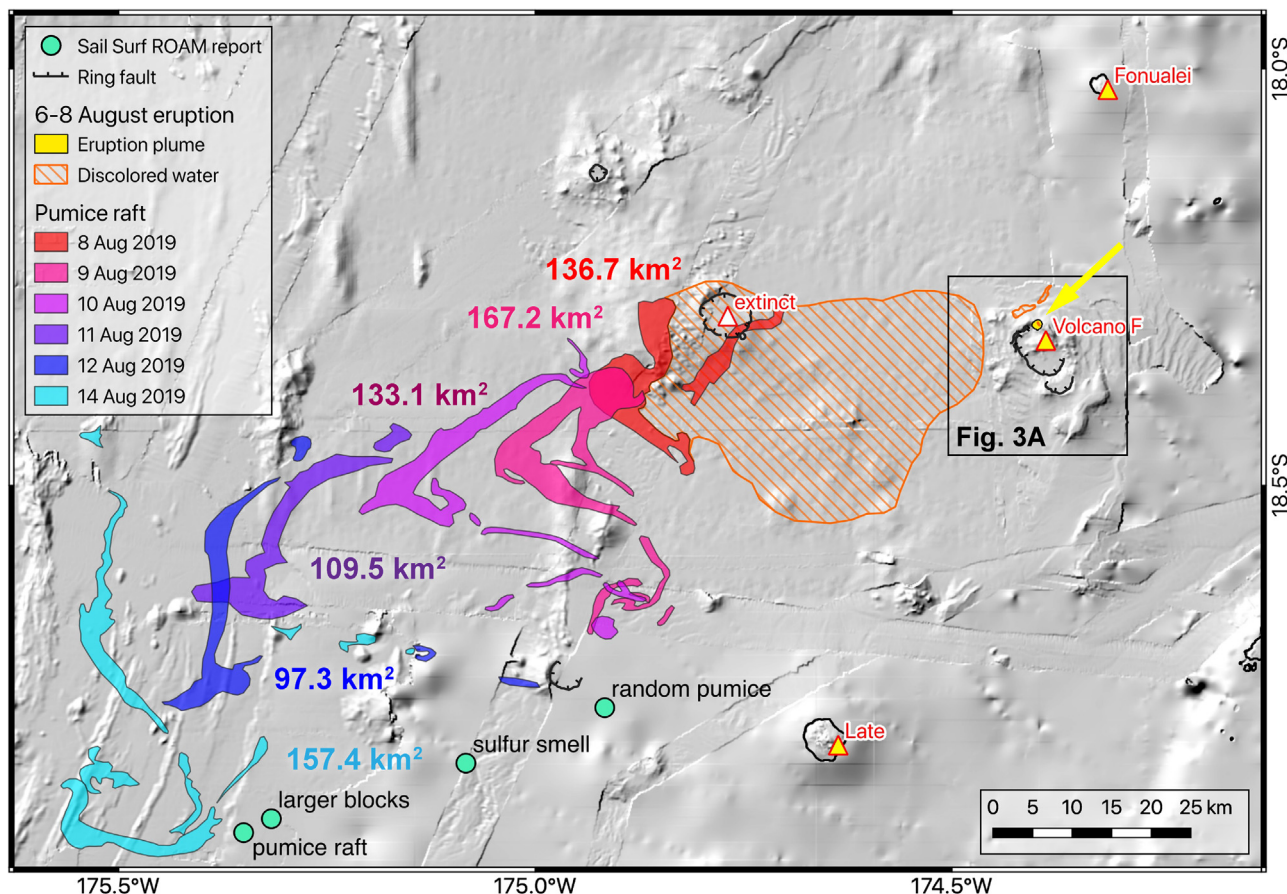


Fig. 2. Extent of discolored water and the pumice raft between the 8 and 14 August 2019 mapped using imagery of NASA's MODIS (NASA, 2019) and ESA's Sentinel-2 satellite. Also shown are the coordinates and the observations of the Sail Surf ROAM report (see text for details) from 15 August 2019. Back-tracing of the pumice raft clearly points towards Volcano F as the most likely origin of the submarine eruption. The yellow arrows points towards the site of eruption imaged in Fig. 3. (For interpretation of the references to colour in this figure legend, the reader is referred to the web version of this article).

We used imagery from ESA's Sentinel-2 satellite to locate the origin of the pumice raft and the actual site of eruption. On images from 6 August 2019, the satellite captured the beginning of the submarine eruption (Fig. 3 A). Two distinct circular eruption plumes are clearly visible on the sea surface: a large one with a diameter of ~ 1.2 km and a smaller one with a diameter of ~ 250 m (Fig. 3B). These two plumes may represent two pulses of the ongoing eruption. Their different sizes could result from progressive expansion of volcanic gases released explosively by two different eruption pulses. Vapor and/or gas possibly exsolving from ejecta and/or erupted pumice appears to be drifting in a northwesterly direction in accordance with the prevailing wind direction at this time ($\sim 140^\circ$ at 35 kmph wind speed; information extracted from <https://earth.nullschool.net>). By 8 August volcanic activity had decreased; Sentinel-2 satellite imagery shows a weak feature at the site of the 6 August eruption plume that either represents small plumes of discolored water or a series of small volcanic cones reaching shallow depths. To the north and northwest, two patches of discolored water are clearly visible and further to the NW traces of pumice can be distinguished (Fig. 3C). However, the larger area of discolored water has already drifted to the west of Volcano F and is captured in imagery from NASA's MODIS satellite. We mapped the extent of the discolored water as of 8 August 2019 along with the pumice raft (Fig. 2). The 6–8 August 2019 eruption of Volcano F can thus be considered as a 2 day-long event. The center of the eruption is located directly on top of Volcano F where the wall of the main caldera intersects with the post-caldera constructional cone complex (Fig. 4).

The mapped area of the pumice raft at the end of the eruption (8 August) was 136.7 km^2 and increased one day later to 167.2 km^2 (Fig. 2). Over the next three days (10–12 August), the raft continuously decreased in size to less than 100 km^2 , potentially as a result of waterlogging or abrasion (cf. Jutzeler et al., 2014). On 14 August, the area of the pumice raft had again increased to 157.4 km^2 (Fig. 2). Initially, the raft drifted westwards, followed by a preferred drift direction to the west-southwest between 8–12 August; The change in drift direction towards the south-southwest on 12–14 August may have enhanced the fragmentation of the raft. At least nine individual raft fragments have been mapped on satellite imagery from 14 August (Fig. 2) and may explain the increase in the overall area of the raft(s) observed between 12–14 August. On 21 August, the remnants of the pumice raft were imaged close to the maritime boundary between Tonga and Fiji (Fig. 1B), and, based on observations of previous pumice rafts (Bryan et al., 2012) is expected to hit the Great Barrier Reef and ultimately the shoreline of Australia in January or February 2020. From the initial size of the pumice raft, we can model the erupted volume and its Dense Rock Equivalent (DRE) following the method of Jutzeler et al. (2014). In our calculations we used average raft thicknesses of 0.1, 0.3 and 0.5 m which corresponds to the extremes of the pumice raft generated by the 2012 eruption of Havre (Jutzeler et al., 2014: 0.1 and 0.5 m thickness at the margins and center of the raft, respectively) and the observed thickness of the August 2019 pumice raft (0.3 m). The estimated minimum erupted volume is $8.2\text{--}41.0 \times 10^6 \text{ m}^3$, which corresponds to $2.7\text{--}12.3 \times 10^6 \text{ m}^3$ DRE (Table 1). This, however, does not take into account any submarine volcanic deposits or volcaniclastic material

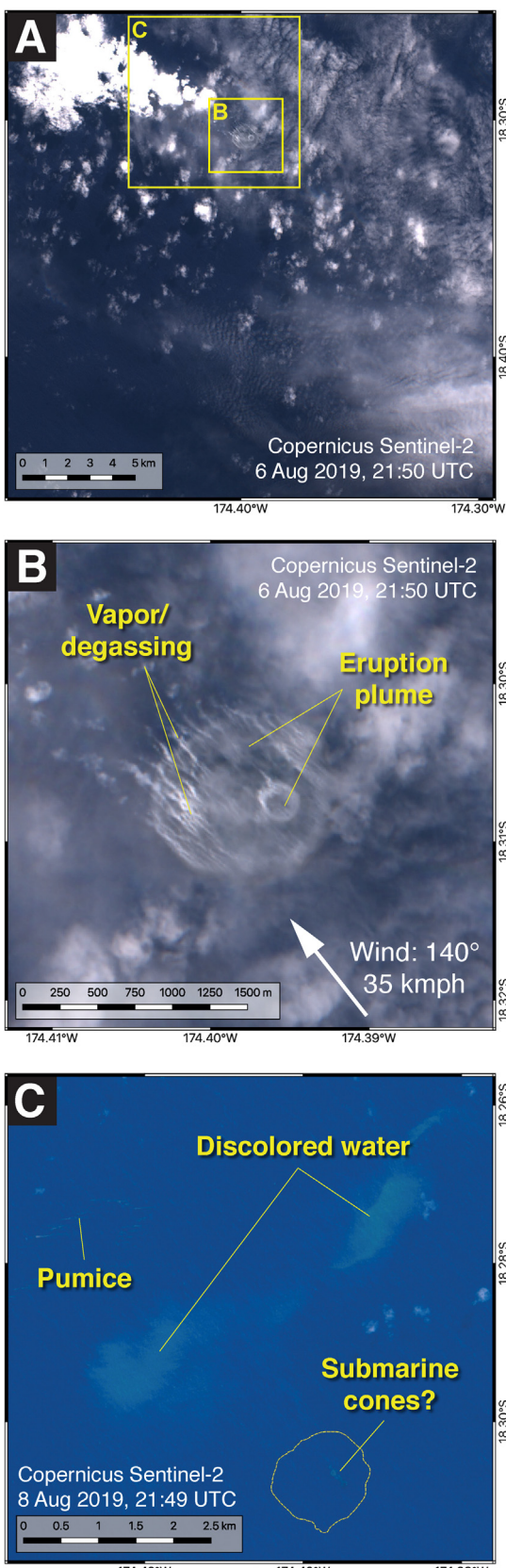


Fig. 3. A) and B) Sentinel-2 satellite image of the eruption on 6 August 2019 (21:59:21 UTC). The submarine eruption plumes are clearly visible on the sea surface and possible gas/vapor released from eruptive products is visible drifting to the NW. C) Sentinel-2 satellite image of the waning eruption on 8 August 2019 (21:49:09 UTC). Discolored water is visible at the eruption site and to the N and NW along with traces of floating pumice. The discolored water at the eruption site could also be interpreted as shallow submarine volcanic cones. The eruption plume

Table 1

Estimates of raft volume, total pumice volume and dense rock equivalent assuming an initial area of the pumice raft of 136.7 km² and the resulting VEI.

| Average thickness | 0.1 m | 0.3 m | 0.5 m |
|-----------------------|------------------------------------|-------------------------------------|-------------------------------------|
| Total raft volume | 0.014 km ³ | 0.041 km ³ | 0.068 km ³ |
| Pumice volume | 8.2*10 ⁶ m ³ | 24.6*10 ⁶ m ³ | 41.0*10 ⁶ m ³ |
| Dense rock equivalent | 2.5*10 ⁶ m ³ | 7.4*10 ⁶ m ³ | 12.3*10 ⁶ m ³ |
| VEI | 2 | 2 | 3 |

dispersed in the atmos- or hydrosphere. Thus, the corresponding minimum Volcanic Explosivity Index (VEI) of the submarine eruption is 2 to 3 (Table 1).

3. Seismicity and T-phases associated with the eruption

In order to further constrain the onset and duration of the volcanic eruption and to infer on potential seismic precursor events to the eruption, we searched for seismic events in the vicinity of Volcano F over the relevant time period. The International Seismological Centre (ISC) Preliminary Bulletin lists a total of eight shallow teleseismic earthquakes within 70 km of the eruption site in the period 1–6 August 2019 (Table 2; Fig. 5). Unfortunately, these events have large location uncertainties of 14–68 km due to large distances from the nearest reporting stations and large azimuth gaps in station coverage (Table 2; Supplementary Fig. 1). Of particular interest is the event at 9:01 UTC on 5 August (id: 201908050901A), which is the strongest and closest to Volcano F. The centroid-moment tensors for this event, available from the Global Centroid Moment Tensor Project (Ekström et al., 2012), locates slightly southeast of Volcano F and indicates an earthquake with significant non-double-couple tensors and a strong vertical pressure axis (Fig. 4). Such focal mechanisms, known as vertical compensated-linear-vector-dipoles, are common to shallow earthquakes associated with active volcanoes and are assumed to be related to magma migration or eruption processes (Shuler et al., 2013). When considering centroid-moment tensors of shallow earthquakes (depth <50 km) in this region over the last 20 years, there are three more compensated-linear-vector-dipole events besides a majority of normal faulting double-couple events (Supplementary Fig. 2). Given the close location to Volcano F, the timing shortly prior to the occurrence of the eruption plume and the specific centroid-moment tensor, which is typical for active volcanoes, we infer that this event (Fig. 5; id: 201908050901A) is related to the eruption of Volcano F. The relation of the seven remaining events to the volcanic eruption is more ambiguous. The preliminary epicenter locations are offset to the west and some are even closer to the extinct volcanic edifice west of Volcano F (Fig. 4). Considering the azimuthal distribution of stations recording the teleseismic events, a gap between ~90°–240° from north is present towards the Southern Pacific region. Seismic rays leaving the hypocenters east (where most stations are located) have travelled through a mantle region of highly heterogeneous P and S velocities (Wei et al., 2015). However, preliminary ISC locations are based on a homogenous earth model (Bondár and Storchak, 2011) and thus a systematic offset in east-west direction of the epicenter locations cannot be ruled out and we cannot unambiguously relate the events to Volcano F.

T-phase signals associated with submarine volcanic activity are a typical phenomenon in the Southwest Pacific (Metz et al., 2019; Talandier and Okal, 1987). We inspected the broadband vertical component seismograms of station RAR (Rarotonga, Cook Islands)

from 6 August is illustrated by the yellow dashed outline. Images contain modified Copernicus Sentinel data 2019. (For interpretation of the references to colour in this figure legend, the reader is referred to the web version of this article).

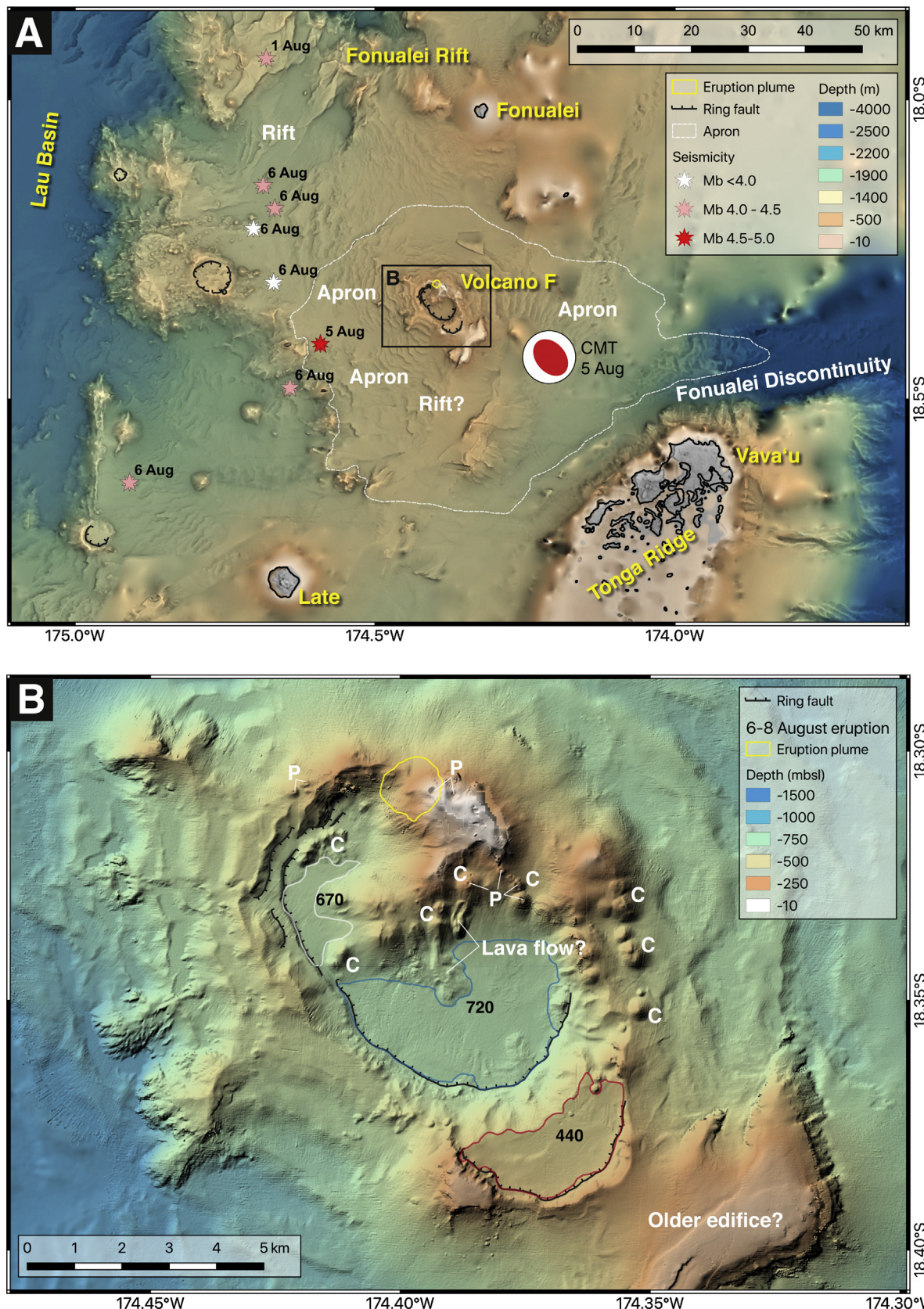


Fig. 4. A) Bathymetric map of the Tofua Arc between Fonualei and Late islands, showing the northern termination of the Tonga Ridge at the Fonualei Discontinuity and the southern termination of the Fonualei Rift. Image enhanced with terrain texture shading (TTS). Epicenters of Table 2 are plotted along with the centroid-moment tensor for the Mb 4.7 event of 5 Aug 2019. B) Detailed bathymetry of Volcano F with the eruption site (yellow circle), the partially preserved caldera floors (at 440, 670 and 720 mbsl) and the ring faults. Young volcanic cones are labelled with 'C' and 'P' denotes pit craters at their top. Note the presence of a potential lava flow and the different depth scale compared to A). No TTS enhancement used in B), hill shading from the NW. The digital elevation model of A) and B) integrates data from the global GMRT grid (version 3.4 of July 2017: [Ryan et al., 2009](#)), RV Southern Surveyor cruise SS2004/11 and RV Sonne cruise SO-267 ([Hannington et al., 2019](#)). The Southern Surveyor Multibeam Echosounder Data downloaded on 29-08-2019 was collected on voyage SS2004/11 by the Marine National Facility. (For interpretation of the references to colour in this figure legend, the reader is referred to the web version of this article).

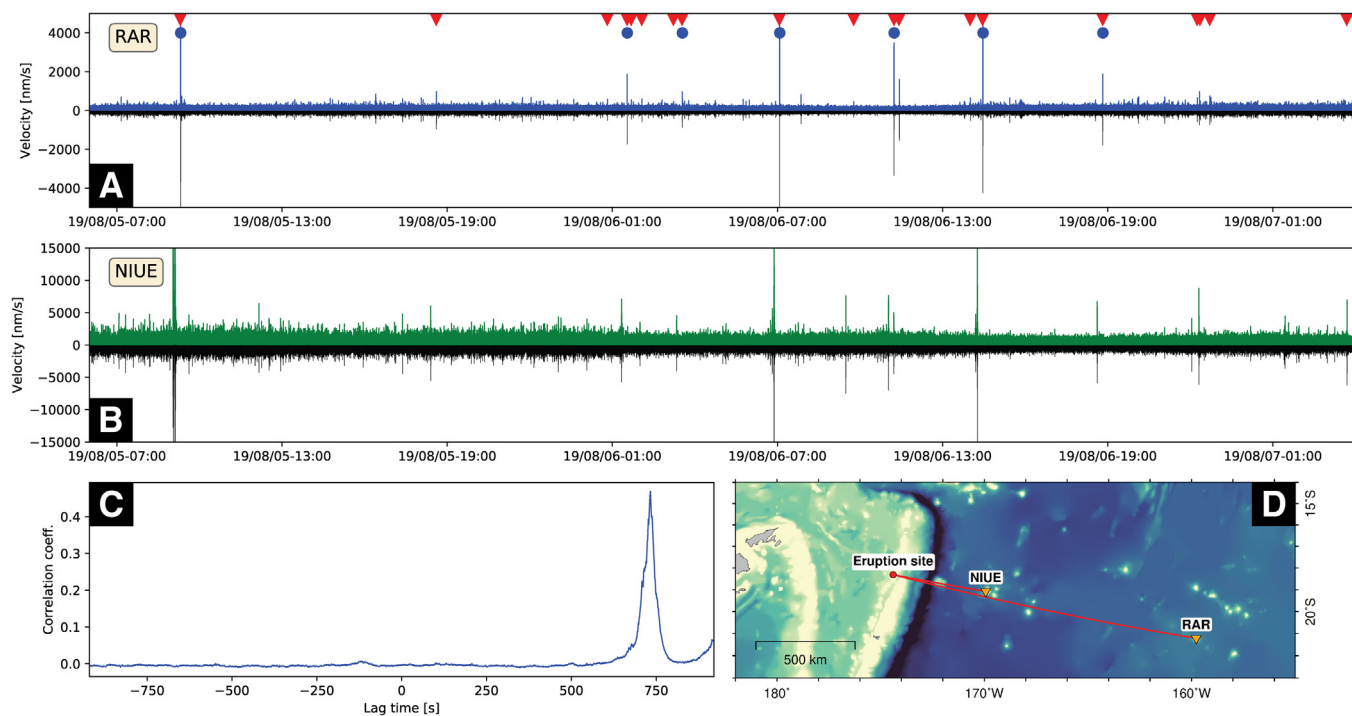


Fig. 5. T-phase data interpreted as originating from the Volcano F eruption site. A) Vertical component seismogram (black) and waveform envelope (blue) of station RAR covering the duration of the eruption. Red triangles at top indicate the onset of individual T-phases that have a lag time of 733 s to station NIUE. Blue dots indicate theoretical T-phase arrivals originating from teleseismic earthquakes located in the vicinity of Volcano F. Epicenters of the teleseismic events are plotted in Fig. 4. B) Seismogram (black) and waveform envelope (green) of station NIUE. C) Cross correlation function for the trace envelope of stations RAR and NIUE for the period displayed above. Note the peak at 733 s lag time, indicating that recorded phases must have arrived from the direction of the eruption site. D) Map showing the location of RAR, NIUE and the eruption site. (For interpretation of the references to colour in this figure legend, the reader is referred to the web version of this article).

and NIUE (Niue Island) to identify T-phases originating from the region of Volcano F. Six-hour long sections of the seismogram-envelope on both stations were cross correlated for the period 1 to 9 Aug 2019. However, it is not possible to perform a unique triangulation of the source with only two stations. Considering the 1,086 km distance between the two stations and assuming a sound velocity of 1.48 km/s in the SOFAR channel of the Southwest Pacific (Denham and Kibblewhite, 1970), T-phases arriving from the direction of Volcano F should have a delay of 733 s on station RAR compared to station NIUE. In the period 5 Aug 2019 9:00 UTC to 7 Aug 2019 4:00 UTC both stations show a good correlation at a lag time of 733 s (Fig. 5C) and we identified a total of 19 individual T-phases which could plausibly have originated at Volcano F (Fig. 5A). Comparing the theoretical T-phase onsets of all teleseismic events in Table 2 (blue dots in Fig. 5A) all of the events coincide with observed T-phase arrivals at station RAR (red triangles in Fig. 5A). Many of those with the largest amplitudes are related to a teleseismic event in the region of Volcano F. In this region, earthquakes of magnitude smaller than ~ 3.5 are likely missing in the ISC Bulletin due to the limited coverage of the global seismograph networks. Thus, T-phase events without a teleseismic equivalent may represent earthquakes below this Mb 3.5 detection threshold. Generally, the signal-to-noise ratio of T-phase events arriving at station RAR is poorer than for T-phases related to volcanic activity at Monowai in the Kermadec Arc (Metz et al., 2019). We propose this difference in T-phase amplitude is at least partially related to the less favorable ray path between Volcano F and station RAR, because the shallow marine to subaerial Tonga Ridge may hinder the transmission of T-phases compared to from Monowai. Nevertheless, we note that the period of most frequent T-phase detections (6 Aug 2019 1:00 until 23:30 UTC) includes the time of a visual record of an ongoing eruption at Volcano F (Fig. 3), supporting the correlation of the increased seismic activity to the eruption.

4. Morphology and geology of Volcano F

In addition to the presented constraints on the dimension and timing of the recent submarine eruption of Volcano F, we here present bathymetric and compositional data of the volcano in order to provide a solid framework for future, more detailed studies. Volcano F is situated in the Tofua arc front about halfway between the volcanic islands of Fonualei to the North and Late to the South (Fig. 4A). The maximum along-arc water depth between these volcanoes is about 1,100 m; Volcano F thus rises over one kilometer from the surrounding seafloor. The edifice is dominated by a 8.7×6 km large caldera that is ~ 670 m and ~ 720 m deep in the northwestern and southeastern sections, respectively (Fig. 4B). The caldera walls are typically between 200–300 m high. At the southeastern margin of this morphologically youngest caldera, another partially preserved caldera floor is present at ~ 440 m (Fig. 4B), indicating a complex, multi-stage evolution of the volcanic edifice. The top of the post-caldera constructional cone complex in the northern half of the caldera was only 35 m below sea level when mapped in 2004. Based on their pristine morphology, several young volcanic cones (labelled 'C' in Fig. 4B) are located on this dome complex, on the northern caldera floor, and outside of the main caldera on the eastern flank of the volcano. Some of these cones appear to be aligned and/or topped by pit craters (labelled 'P' in Fig. 4B). The volcanoclastic apron of Volcano F is characterized by seafloor dipping away from the main edifice with sediment waves (cf. Pope et al., 2018) and low backscatter indicative of a sedimented seafloor. The apron covers a region approximately 50–60 km in diameter and sheds material into the canyon to the east associated with the Fonualei Discontinuity (Fig. 4A). Bathymetric mapping in 2018/19 shows that Volcano F lies at the junction of several cross-cutting structural features. The Fonualei Discontinuity which marks the northern boundary of the Tonga Ridge and runs roughly E-W from

Table 2 Teleseismic earthquakes in the vicinity of the Volcano F in the time span 1–6 August 2019. The f in column five (depth) indicates that hypocentral depths have been fixed for the location inversion but are poorly resolved. Hypocenters have been retrieved from the ISC Preliminary Bulletin (www.isc.ac.uk/iscbulletin/; Bondár and Storchak, 2011).

| Date | Origin time | Lat. | Lon. | Depth [km] | Mag. [mb] | RMS [s] | Semi-major axis of 90% ellipse [km] | Semi-minor axis of 90% ellipse [km] | Azimuth of error ellipse | Number of defining phases | Gap in azimuth coverage | f |
|----------|-------------|-----------|------------|------------|-----------|---------|-------------------------------------|-------------------------------------|--------------------------|---------------------------|-------------------------|--------|
| 01.08.19 | 15:01:29.48 | 17.9316°S | 174.6815°W | 0.0f | 4.1 | 0.80 | 29.7 | 20.6 | 152 | 11 | 143 | 83.03 |
| 05.08.19 | 09:01:01.89 | 18.4083°S | 174.5911°W | 10.0f | 4.7 | 0.80 | 16.3 | 14.2 | 132 | 38 | 44 | 173.66 |
| 06.08.19 | 01:14:36.33 | 18.3056°S | 174.6690°S | 0.0f | 3.9 | 0.77 | 41.2 | 22.7 | 145 | 8 | 124 | 147.54 |
| 06.08.19 | 03:14:43.55 | 18.2157°S | 174.7027°W | 0.0f | 3.9 | 0.48 | 38.4 | 35.2 | 67 | 5 | 168 | 85.44 |
| 06.08.19 | 06:47:03.84 | 18.1820°S | 174.6671°W | 0.0f | 4.1 | 0.77 | 28.6 | 16.6 | 138 | 16 | 124 | 157.12 |
| 06.08.19 | 10:56:21.41 | 18.4813°S | 174.6418°W | 0.0f | 4.1 | 0.94 | 29.1 | 21.5 | 130 | 10 | 138 | 92.45 |
| 06.08.19 | 14:10:10.26 | 18.1435°S | 174.6886°W | 0.0f | 4.2 | 0.85 | 23.7 | 17.8 | 130 | 20 | 121 | 41.64 |
| 06.08.19 | 18:31:31.14 | 18.6396°S | 174.9092°W | 0.0f | 4.2 | 0.85 | 63.8 | 36.6 | 31 | 5 | 221 | 47.77 |

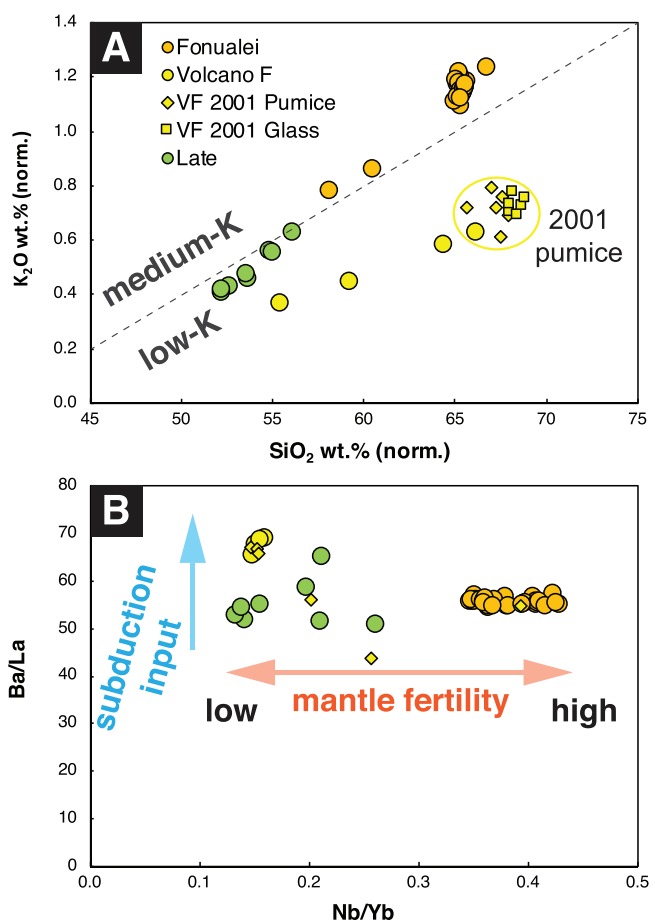


Fig. 6. A) K₂O versus SiO₂ (both in wt.%, volatile-free and normalized to a total of 100 wt.%) diagram after Le Maitre et al. (1998). B) Ba/La versus Nb/Yb. VF stands for Volcano F and shows pumice data (whole rock and glass analyses) of the 2001 eruption (Bryan et al., 2004). Based on their trace element composition, some pumice clasts may originate from volcanic sources other than Volcano F. Data compiled from Hammond (2006); Turner et al. (2012), Beier et al. (2017), and Bryan et al. (2004).

the forearc into the Tofua Arc basement (Fig. 4A). The Fonualei Rift which is propagating southwards, and northeast-southwest orientated rifting southwest of the Fonualei Rift tip (Fig. 4A). Structures to the north of Volcano F appear to be extensional whereas two centroid-moment tensors south of the volcano indicate compression (Supplementary Fig. 2).

Volcanic rocks dredged from Volcano F range from basaltic andesite to dacite (cf. Dale et al., 2012; Hammond, 2006) as do those on the adjacent arc volcanoes of Fonualei and Late. However, the low-K series lavas of Volcano F are different to the adjacent volcanoes whose lavas plot on (Late) or above (Fonualei) the low-K to medium-K dividing line (Fig. 6A). Pumice clasts collected onshore from the 2001 eruption of Volcano F are dacitic (Bryan et al., 2004) and slightly more silicic than dredged lavas (Fig. 6A). Furthermore, lavas collected from within the Volcano F caldera generally have lower silica contents (dredges ND25 and ND29 have 59.1 and 54.5 wt.% SiO₂, respectively) than those dredged from the post-caldera constructional cone complex (ND28 and ND30 with 64.2–66.0 wt.% SiO₂: Hammond, 2006). Thus, magma differentiation in crustal magma chambers may play the dominant role for the magmatic evolution of Volcano F. In terms of mantle source, Volcano F has a high-Ca boninitic magmatic heritage whereas lavas from Late island are incompatible element depleted basaltic (Cooper et al., 2010). In both cases the refractory and incompatible element depleted geochemical character results from derivation from a mantle wedge that has undergone various extents of melt

depletion in the backarc prior to melting underneath the arc volcanic front. Consistently, lavas from Volcano F are likely derived from a more refractory mantle source than those from Late or Fonualei islands if we consider the Nb/Yb ratio (Fig. 6B) as a measure for the fertility of the mantle wedge (cf. Brandl et al., 2017). In turn, Volcano F lavas indicate a relatively high contribution from subduction fluids based on their high Ba/La (Fig. 6B).

5. Conclusion and future directions

Combined observations from satellite remote sensing, a series of telesismically detected earthquakes, associated T-phase events, and new bathymetric data provide a clear image of the submarine VEI 2–3 eruption of Volcano F in the Tofua Arc of Tonga between the 6 and 8 August 2019. The eruption produced large amounts of pumice indicating a dacitic or even rhyolitic composition of the 2019 eruption products. The previous eruption of dacite (but not rhyolite) is evident from geochemical analyses of lavas dredged in 2004 and pumice erupted from Volcano F in 2001. Hence, future petrological-geochemical studies of the 2019 eruption products are required. The range of lava compositions (basaltic andesite to dacite) indicates a composite edifice of Volcano F with a mafic caldera stage and a more silicic post-caldera constructional cone complex. Two caldera generations, one partially preserved with a floor at 440 m and the other, younger central caldera at ~700 m water depth, and the large post-caldera cone complex with several clusters of individual volcanic cones, some with pit craters and possibly lava flows are further evidence of the complex evolution of Volcano F. Recent multibeam mapping indicates substantial volcanoclastic output of the volcano as reflected by the large apron with >50 km diameter. Seismic precursor events were detected in the hours to days leading up to the first visual observation of the eruption on 6 August. Future high-resolution mapping of Volcano F will be required to better interpret the structure of the volcano and its tectonic setting. Detailed visual surveying, sampling and petrological-geochemical studies are required to further constrain the current state and the general dynamics of the magmatic plumbing system of this major and potentially hazardous arc volcano.

Declaration of interests

The authors declare that they have no known competing financial interests or personal relationships that could have appeared to influence the work reported in this paper.

Acknowledgments

We would like to thank the master, the crew and the shipboard scientific party of RV Sonne expedition SO-267. Funding of this cruise through the German Federal Ministry of Education and Research (BMBF) is acknowledged (BMBF 03S0575). We acknowledge the constructive reviews by William Chadwick and an anonymous reviewer. MS acknowledges funding by Metal Earth. We further acknowledge the IRIS archives from which the seismological data were retrieved and the agencies operating the stations. The IRIS data services are funded by National Science Foundation Agreement EAR-1261681. Seismic data have been processed with the ObsPy open source toolbox (Krischer et al., 2015). This is Metal Earth contribution MERC-ME-2019-224.

Appendix A. Supplementary data

Supplementary material related to this article can be found, in the online version, at doi:<https://doi.org/10.1016/j.jvolgeores.2019.106695>.

References

- Arculus, R.J., SS2004/11 shipboard scientists, 2004. SS11/2004 Voyage Summary: NoToVE-2004 (Northern Tonga Vents Expedition): submarine hydrothermal plume activity and petrology of the northern Tofua Arc, Tonga. Downloaded on 27 August 2019: https://www.cmar.csiro.au/data/reporting/get_file.cfm?ev_pub_id=901.
- Beier, C., Turner, S.P., Haase, K.M., Pearce, J.A., Münker, C., Regelous, M., 2017. Trace element and isotope geochemistry of the northern and Central Tongan Islands with an emphasis on the genesis of high Nb/Ta signatures at the northern volcanoes of Tafahi and niuatoputapu. *J. Petrol.*, <http://dx.doi.org/10.1093/petrology/egx047>.
- Bondár, I., Storchak, D., 2011. Improved location procedures at the international seismological centre. *Geophys. J. Int.* 186 (3), 1220–1244, <http://dx.doi.org/10.1111/j.1365-246X.2011.05107.x>.
- Brandl, P.A., Hamada, M., Arculus, R.J., Johnson, K., Marsaglia, K.M., Savov, I.P., Ishizuka, O., Li, H., 2017. The arc arises: the links between volcanic output, arc evolution and melt composition. *Earth Planet. Sci. Lett.* 461, 73–84, <http://dx.doi.org/10.1016/j.epsl.2016.12.027>.
- Bryan, S.E., Cook, A., Evans, J.P., Colls, P.W., Wells, M.G., Lawrence, M.G., Jell, J.S., Greig, A., Leslie, R., 2004. Pumice rafting and faunal dispersion during 2001–2002 in the Southwest Pacific: record of a dacitic submarine explosive eruption from Tonga. *Earth Planet. Sci. Lett.* 227, 135–154, <http://dx.doi.org/10.1016/j.epsl.2004.08.009>.
- Bryan, S.E., Cook, A.G., Evans, J.P., Hebden, K., Hurrey, L., Colls, P., Jell, J.S., Weatherley, D., Firth, J., 2012. Rapid, long-distance dispersal by pumice rafting. *PLoS One* 7, e40583, <http://dx.doi.org/10.1371/journal.pone.0040583.g001>.
- Chadwick, W.W., Wright, I.C., Schwarz-Schampera, U., Hyvernaud, O., Reymond, D., de Ronde, C.E.J., 2008. Cyclic eruptions and sector collapses at Monowai submarine volcano, Kermadec arc: 1998–2007. *Geochim. Geophys. Geosystems* 9, Q10014, <http://dx.doi.org/10.1029/2008GC002113>.
- Chadwick Jr, W.W., 2019. Recent eruptions between 2012 and 2018 discovered at west mata submarine volcano (NE Lau Basin, SW Pacific) and characterized by new ship, AUV, and ROV data. *Front. Mar. Sci.* 6, 495, <http://dx.doi.org/10.3389/fmars.2019.00495>.
- Cooper, L.B., Plank, T., Arculus, R.J., Hauri, E.H., Hall, P.S., Parman, S.W., 2010. High-Ca boninites from the active Tonga Arc. *J. Geophys. Res.*, <http://dx.doi.org/10.1029/2009jb006367>.
- Crisp, J., 1984. Rates of magma emplacement and volcanic output. *J. Volcanol. Geotherm. Res.* 20, 177–211.
- Dale, C.W., Macpherson, C.G., Pearson, D.G., Hammond, S.J., Arculus, R.J., 2012. Inter-element fractionation of highly lithophile elements in the Tonga Arc due to flux melting of a depleted source. *Geochim. Cosmochim. Acta* 89, 202–225, <http://dx.doi.org/10.1016/j.gca.2012.03.025>.
- Denham, R.N., Kibblewhite, A.C., 1970. The sound-velocity structure of the South Pacific Ocean. *New Zealand J. Geol. Geophys.* 13 (1), 39–51, <http://dx.doi.org/10.1080/00288306.1970.10428205>.
- Ekström, G., Nettles, M., Dziwoński, A.M., 2012. The global CMT project 2004–2010: Centroid-moment tensors for 13,017 earthquakes. *Phys. Earth. Plan. Interniors* 200–201, 1–9, <http://dx.doi.org/10.1016/j.pepi.2012.04.002>.
- Global Volcanism Program, 2013. Unnamed (243091) in *Volcanoes of the World*, v. 4.8.2. Venzke, E. (ed.). Smithsonian Institution. Downloaded 29 Aug 2019: <https://volcano.si.edu/volcano.cfm?vn=243091>.
- Global Volcanism Program, 2019. Report on unnamed (Tonga). In: Sennert, S.K. (Ed.), *Weekly Volcanic Activity Report*. Smithsonian Institution and US Geological Survey, 14 August–20 August 2019.
- Hammond, S., PhD thesis 2006. *Lithium and Li Isotopes As Tracers of Subduction Zone Processes*. Open University, 255 pp.
- Hannington, M. D., Kopp, H., Schnabel, M., 2019. RV SONNE Fahrbericht / Cruise Report SO267: ARCHIMEDES I: Arc Rifting, Metallogeny and Microplate Evolution – an Integrated Geodynamic, Magmatic and Hydrothermal Study of the Fonualei Rift System, NE Lau Basin, Suva (Fiji) – Suva (Fiji), 11.12.2018–26.01.2019. GEOMAR Report, N. Ser. 049. GEOMAR Helmholtz-Zentrum für Ozeanforschung Kiel, Kiel, Germany, 49 pp. <https://doi.org/10.3289/GEOMAR.REP.NS.49.2019>.
- Jutzeler, M., Marsh, R., Carey, R.J., White, J.D.L., Talling, P.J., Karlstrom, L., 2014. On the fate of pumice rafts formed during the 2012 Havre submarine eruption. *Nat. Commun.* 5, 3660, <http://dx.doi.org/10.1038/ncomms4660>.
- Krischer, L., Megies, T., Barsch, R., Beyreuther, M., Lecocq, T., Caudron, C., Wassermann, J., 2015. ObsPy: a bridge for seismology into the scientific Python ecosystem. *Comput. Sci. Discov.* 8, 14003, <http://dx.doi.org/10.1088/1749-4699/8/1/014003>.
- Le Maître, R.W., Streckeisen, A., Zanettin, B., Le Bas, M.J., Bonin, B., Bateman, P., Belini, G., Dudek, A., Efremova, S., Keller, J., Laméryre, J., Sabine, P.A., Schmid, R., Sorensen, H., Woolley, A.R., 1998. *Igneous Rocks – a Classification and Glossary of Terms*, 2nd ed. Cambridge University Press, Cambridge.
- Mantas, V.M., Pereira, A.J.S.C., Morais, P.V., 2011. Plumes of discolored water of volcanic origin and possible implications for algal communities. The case of the Home Reef eruption of 2006 (Tonga, Southwest Pacific Ocean). *Remote Sens. Environ.* 115, 1341–1352, <http://dx.doi.org/10.1016/j.rse.2011.01.014>.
- Metz, D., Watts, A.B., Grevemeyer, I., Werner, R., Huusmann, H., 2019. Updated seafloor topography and T phase seismicity at Monowai, northern Kermadec Arc. *New Zealand J. Geol. Geophys.* 0, 1–6, <http://dx.doi.org/10.1080/00288306.2019.1651747>.
- Metz, D., Watts, A.B., Grevemeyer, I., Rodgers, M., Paulatto, M., 2016. Ultra-long-range hydroacoustic observations of submarine volcanic activity at Monowai,

- Kermadec Arc. Geophys. Res. Lett. 43, 1529–1536, <http://dx.doi.org/10.1002/2015GL067259>.
- NASA (2019): <https://worldview.earthdata.nasa.gov/?v=-175.42198623135474,-19.021735394030717,-173.66686787395471,-17.828196260427024&t=2019-08-08-T04%3A50%3A46Z>.
- Pope, E.L., Jutzeler, M., Cartigny, M.J.B., Shreeve, J., Talling, P.J., Wright, I.C., Wysoczanski, R.J., 2018. Origin of spectacular fields of submarine sediment waves around volcanic islands. Earth Planet. Sci. Lett. 493, 12–24, <http://dx.doi.org/10.1016/j.epsl.2018.04.020>.
- Resing, J.A., Rubin, K.H., Embley, R.W., Lupton, J.E., Baker, E.T., Dziak, R.P., Baumberger, T., Lille, M.D., Huber, J.A., Shank, T.M., Butterfield, D.A., Clague, D.A., Keller, N.S., Merle, S.G., Buck, N.J., Michael, P.J., Soule, A., Caress, D.W., Walker, S.L., Davis, R., Cowen, J.P., Reysenbach, A.-L., Thomas, H., 2011. Active submarine eruption of boninite in the northeastern Lau Basin. Nat. Geosci. 4, 799–806, <http://dx.doi.org/10.1038/ngeo1275>.
- Ryan, W.B.F., Carbotte, S.M., Coplan, J.O., O'Hara, S., Melkonian, A., Arko, R., Weissel, R.A., Ferrini, V., Goodwillie, A., Nitsche, F., Bonczkowski, J., Zemsky, R., 2009. Global multi-resolution topography synthesis. Geochim. Geophys. Geosystems 10, Q03014, <http://dx.doi.org/10.1029/2008GC002332>.
- Shuler, A., Nettles, M., Ekström, G., 2013. Global observations of vertical-CLVD earthquakes at active volcanoes. J. Geophys. Res. Solid Earth 118, 138–164, <http://dx.doi.org/10.1029/2012JB009721>.
- Smith, I.E.M., Price, R.C., 2006. The Tonga–kermadec arc and Havre–lau back-arc system: their role in the development of tectonic and magmatic models for the western Pacific. J. Volcanol. Geotherm. Res. 156, 315–331, <http://dx.doi.org/10.1016/j.jvolgeores.2006.03.006>.
- Talandier, J., Okal, E.A., 1987. Seismic detection of underwater volcanism: the example of French Polynesia. Pure Appl. Geophys. 125 (6), 919–950, <http://dx.doi.org/10.1007/BF00879361>.
- Turner, S.P., Caulfield, J., Rushmer, T., Turner, M., Cronin, S., Smith, I.A., Handley, H., 2012. Magma evolution in the primitive, intra-oceanic Tonga arc: rapid petrogenesis of dacites at Fonualei Volcano. J. Petrol. 53, 1231–1253, <http://dx.doi.org/10.1093/petrology/egs005>.
- Vaughan, R.G., Abrams, M., Hook, S.J., Pieri, D.C., 2007. Satellite observations of new volcanic island in Tonga. EOS 88, 37–41.
- Wei, S.S., Wiens, D.A., Zha, Y., Plank, T., Webb, S.C., Blackman, D.K., Dunn, R.A., Conder, J.A., 2015. Seismic evidence of effects of water on melt transport in the Lau back-arc mantle. Nature 518, 395–398, <http://dx.doi.org/10.1038/nature14113>.
- Wright, I.C., Chadwick Jr, W.W., de Ronde, C.E.J., Reymond, D., Hyvernaud, O., Generich, H.-H., Stoffers, P., Mackay, K., Dunkin, M.A., Bannister, S.C., 2008. Collapse and reconstruction of Monowai submarine volcano, Kermadec arc, 1998–2004. J. Geophys. Res. 113 (17), <http://dx.doi.org/10.1029/2007JB005138>, 995–13.